Catalysis Science & Technology

PAPER

View Article Online
View Journal

Cite this: DOI: 10.1039/c4cy01231c

The relationship between the surface oxygen species and the acidic properties of mesoporous metal oxides and their effects on propane oxidation†

Shu Chen, Yanhua Li, Fei Ma, Fang Chen and Weimin Lu*

Received 22nd September 2014,
Accepted 4th November 2014

DOI: 10.1039/c4cy01231c

www.rsc.org/catalysis

The V, Cu and Mo catalysts change the surface oxygen species of *meso*-Mn_2O_3 and these have been used in the oxidation of propane. The oxygen species on the different catalysts were studied in detail, including *in situ* IR of propane under aerobic and anaerobic conditions, X-ray photoelectron spectroscopy (XPS) and *in situ* IR of CO_2 adsorption. The *in situ* IR experiments of NH_3 showed changes in the Lewis and Brønsted acids on the catalysts. We discuss the relationship between the acidic properties and the oxygen species. The results showed that the performance of the catalysts was significantly affected by the different oxygen species.

1 Introduction

Effective catalysts for deep oxidation (combustion) and selective oxidation are urgently needed because of environmental and industrial concerns. The deep oxidation catalysts mainly include manganese oxides, such as Mn_2O_3, which are used for the total oxidation of organic compounds[1–6] owing to their high activity and high mobility of the lattice oxygen.[7–9] Recently, the modified Mn_2O_3 catalysts have gradually been applied to the selective oxidation of light alkanes due to their surface oxygen properties.[10]

The surface chemistry of Mn_2O_3 materials, especially their surface oxygen species, is a very important factor that affects their utility as absorbents, catalysts and/or catalyst supports. Catalyst selectivity is largely governed by the nature of the surface oxygen species.[11–13] These same authors explained that the catalytic reaction occurs mainly due to the effect of the lattice oxygen and adsorbed oxygen. Other authors[1] considered that active surface oxygen species could equally be nucleophilic (O^{2-}) or electrophilic ($O^{<2-}$) and suggested the use of Lewis acid sites (Mn^{+}) to initiate the activation of C–H bonds and the involvement of nucleophilic O^{2-} surface species in total oxidation reactions. Thus far, the study of the role of the surface oxygen species in catalytic oxidation reactions is still controversial.

The acid properties are also taken seriously in the catalytic reaction like the oxygen species, but there is also a debate about the role of acidity. For propane oxidation, many authors believe that the acid property is a key factor for the catalytic activity. In the selective oxidation of propane to propylene, some authors reported that the amount of acid influenced the propane conversion, and the Brønsted acid affected the selectivity of propylene.[14] Many reports considered the acid properties to be significant and used high surface area supports like SBA-15 and *meso*-Al_2O_3 to load several different elements, including Mo and V, to adjust the acidity of the catalysts, but ignored the reasons behind the acid changes.[15,16] Therefore, it is favorable to enhance catalytic properties by adjusting catalyst acidity.

The synthesis and properties of bulk-Mn_2O_3 materials have been intensively studied. Our group synthesized *meso*-Mn_2O_3 to improve the dispersion of some elements and to adjust the acidity of the catalysts and thus the distribution of the surface oxygen species. We loaded V, Cu and Mo on *meso*-Mn_2O_3 because V activates the α-H of propane and is acidic, Cu is an element that undergoes total oxidation, and Mo also activates the α-H of propane but is not as acidic as V. Here we study the influence of the different acidic properties of the catalysts on the oxidation of propane and explore the relationship between the acid properties and the different oxygen species. Our goal is to understand propane oxidation by using the different catalysts.

2. Experimental

2.1 Catalyst preparation

Ordered mesoporous silica with cubic *Ia3d* symmetry (KIT-6) was prepared from TEOS, P_{123} ($EO_{20}PO_{70}EO_{20}$, MW = 5800), butanol, and HCl at 308 K.[17]

Institute of Catalysis, Zhejiang University (Xixi Campus), Hangzhou 310028, PR China. E-mail: luweimin@zju.edu.cn

† Electronic supplementary information (ESI) available. See DOI: 10.1039/c4cy01231c

In a typical synthesis of ordered mesoporous Mn_2O_3 (*meso*-Mn_2O_3), 1 g of KIT-6 was added in 50 mL of acetone. After stirring at room temperature for 2 h, 2 mL of $Mn(NO_3)_2$ solution (C = 5.2446 mol L^{-1}) was added slowly under stirring. After stirring overnight, filtering and drying at room temperature, a dry powder was obtained, followed by calcination at 873 K for 3 h and removal of silica using 2 M NaOH solution in water. After washing with water and drying at 333 K, *meso*-Mn_2O_3 was finally obtained.[18]

For comparison, bulk-Mn_2O_3 was synthesized by thermal decomposition of $MnCO_3$. In a typical run, an equal volume and concentration of Na_2CO_3 and $MnCl_2$ were mixed and stirred for 30 min. After washing and filtering, the precipitate was dried at 373 K, and the resulting white powder ($MnCO_3$) was then calcined at 873 K in air for 4 h with a ramping rate of 2 K min^{-1}.

The introduction of various elements such as V, Mo, and Cu in the *meso*-Mn_2O_3 samples (MO_X–Mn_2O_3) was performed by impregnation of *meso*-Mn_2O_3 with ammonium metavanadate, ammonium molybdate, and copper nitrate as the precursor, respectively. After stirring overnight, the catalyst was dried at 338 K for 12 h and calcined at 623 K in air for 3 h with a ramping rate of 2 K min^{-1}.

2.2. Catalyst characterization

The N_2 sorption isotherms were recorded on a TriStar II 3020 instrument at 77 K. Before measurement, the samples were evacuated at 473 K for 2 h. The specific surface area was determined by the Brunauer–Emmett–Teller (BET) method. For high-resolution transmission electron microscopy (HRTEM), a JEOL-135 2010F TEM at an accelerating voltage of 200 kV was used. To prepare the TEM samples, a dilute particle–ethanol colloidal mixture was ultrasonicated for 30 min and a drop of the solution was placed on a carbon-coated Cu TEM grid. Powder XRD patterns of the samples were obtained with an X-ray diffractometer (XRD, Rigaku-D/Max-B automated powder X-ray diffractometer) operating at 45 kV and 40 mA using Cu Kα radiation (λ = 0.15418 nm). The crystal phase was obtained by wide-angle scanning in the range 10–80° and low-angle scanning in the range 0.5–10°.

IR spectra were recorded on a BioRad, FTS-40A FT-IR spectrophotometer with an IR cell equipped with CaF_2 windows connected to a vacuum dosing system. The catalyst powder was pressed into a self-supporting disc and activated at 200 °C under vacuum for 1 h before the adsorption experiments. *In situ* IR spectra of propane, propylene, and propane/O_2 gaseous species were recorded under vacuum or 5% O_2/He at elevated temperature after the gas phase components in the IR cell were removed by evacuation. The spectrum of the adsorbed species was referenced to the background spectrum of the pretreated catalyst recorded under vacuum at the same temperature before the introduction of adsorbents. Because propane is inert, a slightly different protocol was used. A gas mixture of propane/oxygen was added to the catalyst at 323, 373, 423, 473 and 523 K. We then recorded the spectrum at each temperature.

For the IR spectra of NH_3 or CO_2, all catalysts were pretreated under vacuum at 300 °C for 1 h and chemisorbed under NH_3 or CO_2 when the sample was cooled to room temperature. Adsorption of NH_3 was performed at room temperature (rt), followed by evacuation to remove the adsorbed NH_3. Adsorption of CO_2 was performed at room temperature for 1 h, followed by increasing the temperature to 323, 373, 423, 473, 523 and 573 K. Evacuation and stabilization times at each temperature were 20 min. The signal of NH_3 or CO_2 desorption was analyzed by IR spectroscopy.

X-ray photoelectron spectroscopy (XPS) experiments used a Thermo ESCALAB 250 system with Al Kα radiation (1486.6 eV). The X-ray anode operated at 150 W, and the binding energies were calibrated using the C1s line as a standard (284.8 eV).

2.3. Catalytic performance

The oxidation of propane was carried out in a tubular, fixed bed flow quartz reactor (i.d. 7.4 mm, 270 mm long) under atmospheric pressure. 0.2 g of the catalyst was used to test the catalytic performance. The feedstock C_3H_8/O_2 had a molar ratio of 1.0 at GHSV = 4500 ml $(g\ h)^{-1}$ and reaction temperature of 480 °C. The products and reactants were analyzed by a dual channel on-line gas chromatograph equipped with both TCD and FID and Porapak QS (4.0 m × 1/8 in) and TDX-01 (2.0 m × 1/8 in) columns.

3 Results and discussion

3.1. *Meso*-Mn_2O_3 characterization

Fig. 1A shows a TEM image of KIT-6 exhibiting a very ordered mesostructure. Fig. 1B shows a TEM image of *meso*-Mn_2O_3 also exhibiting an ordered mesostructure. These results

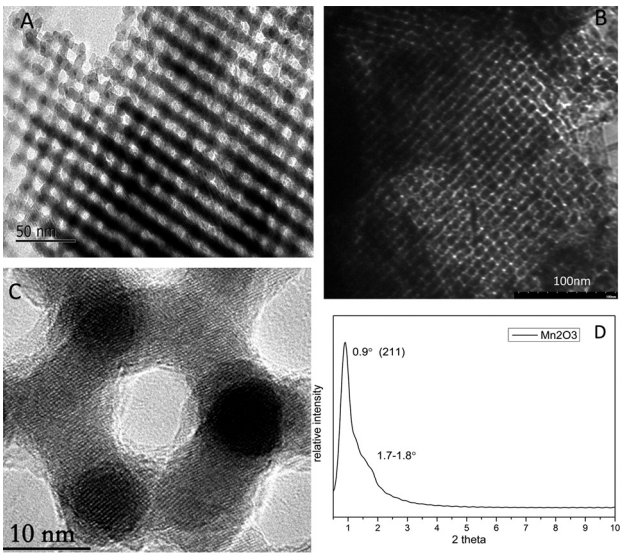

Fig. 1 TEM images of (A) KIT-6 and (B) *meso*-Mn_2O_3. HRTEM image of (C) *meso*-Mn_2O_3 and low-angle XRD patterns of (D) *meso*-Mn_2O_3.

suggest that the mesostructure of *meso*-Mn_2O_3 is well templated from the mesostructure of KIT-6. The HRTEM image (Fig. 1C) of the sample clearly exhibits hexagonally cubic close-packed mesopores with crystalline walls. The low-angle powder X-ray diffraction pattern (Fig. 1D) of the sample shows one sharp peak at ~0.9° and a broad peak at 1.7–1.8°, in good agreement with those of the $Ia\bar{3}d$ space group. These results confirm that the *meso*-Mn_2O_3 crystals have an ordered mesostructure.

Fig. 2 shows the wide-angle XRD patterns of *meso*-Mn_2O_3, exhibiting characteristic peaks associated with α-Mn_2O_3 (JCPDS no. 73-1826), where Mn(III) cations are surrounded by six oxygen atoms forming a distorted octahedron.[19] Similarly, bulk-Mn_2O_3 is also crystalline α-Mn_2O_3. In addition, any metal oxide phase, except for α-Mn_2O_3, cannot be observed in Cu–Mn_2O_3, V–Mn_2O_3 and Mo–Mn_2O_3, even if the metal loading is at 10%. This phenomenon suggests that the metal species are well dispersed on *meso*-Mn_2O_3. Furthermore, the Raman spectra of the samples (Fig. S1†) show that there is a little oligomer of V and Mo species, while Cu species are highly dispersed. HAADF-STEM and elemental mapping images (Fig. S2A and S2B†) prove the good dispersion of V and Mo on *meso*-Mn_2O_3.

Fig. 3 shows the nitrogen sorption isotherms of the samples, showing a typical type IV adsorption. The Brunauer–Emmett–Teller (BET) surface area of KIT-6 is 614 $m^2\ g^{-1}$, but the surface area of *meso*-Mn_2O_3 is much smaller (81 $m^2\ g^{-1}$). After the introduction of various elements, such as V, Mo, and Cu, the surface areas of the samples are further reduced, as summarized in Table 1. The pore size distributions, calculated from the desorption isotherms, exhibit a narrow distribution centered at 6.6 nm for mesoporous KIT-6 and a bigger pore size (8.2 nm) for *meso*-Mn_2O_3. The pore size of the supported catalysts is centered near 7 nm, which is smaller than that of *meso*-Mn_2O_3.

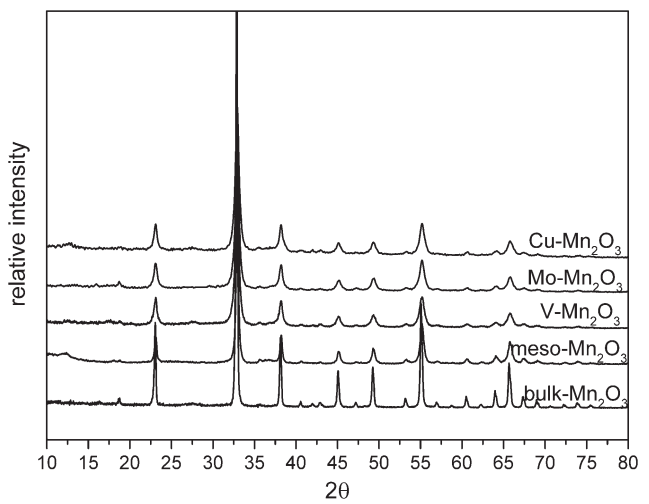

Fig. 2 Wide-angle XRD patterns of bulk-Mn_2O_3, *meso*-Mn_2O_3 and supported catalysts.

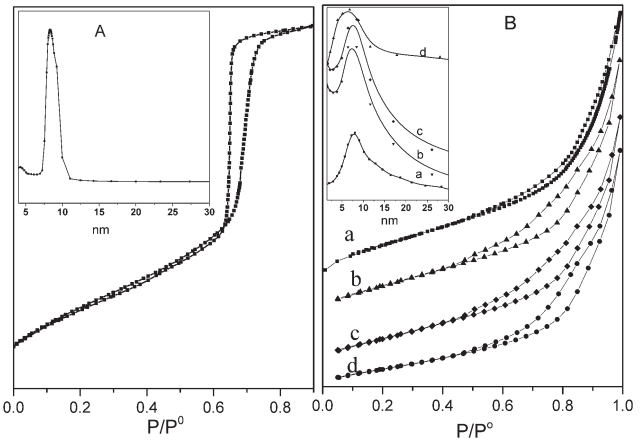

Fig. 3 N_2 sorption isotherms and average pore size distribution of (A) KIT-6 and (B) catalysts: (a) *meso*-Mn_2O_3, (b) Cu–Mn_2O_3, (c) Mo–Mn_2O_3, (d) V–Mn_2O_3.

3.2 Catalytic tests in propane oxidation

Table 2 (Table S1†) presents the catalytic data for propane oxidation reaction performance of the different catalysts. Notably, they have similar conversion, but their product selectivities are quite distinguishable. Propane on *meso*-Mn_2O_3 underwent a deep oxidation reaction, yielding CO_2 (sel. 58.2%) as the main product as well as ethylene (sel. 20.6%). All of the loaded catalysts were compared with *meso*-Mn_2O_3 in the following. After loading 10% CuO, the ethylene selectivity decreased (12.2%), while propylene, as the selective oxidation product of propane, selectivity increased (29.5%) and CO_2 selectivity remained 50%. After loading 10% MoO_3, the propylene selectivity (37.2%) increased, and the cleavage product ethylene decreased, while CO_2 is predominant and little CO was noted. The 10% V_2O_5 underwent selective oxidation of propane and gave propylene as the primary product (sel. 51%). Because of these different products, we suggest that the catalysts have different reaction pathways.

The catalytic performance was measured at V loading levels of 1‰ to 15% to study the influence of the different loading levels on the catalytic activity. The propane conversion is ranging from 24.4 to 28.8%. Increasing the V loading has no impact, except when the V loading level is at 15%. The selectivity of propylene increases from 17.4 to 51.0% with 10% V. Concurrently, the CO_2 selectivity drops greatly and CO rises.

3.3 *In situ* IR analysis

The catalysts exhibited different catalytic activities after the different elements were loaded. To understand the possible reaction pathways for the oxidation of propane, the surface species formed by adsorption of the reactant (propane) and the reaction products (propylene), as well as the transformation of these species on the catalysts were studied by IR spectroscopy using both vacuum and different reaction atmospheres as well as temperature change.

Table 1 Surface areas and average pore width (nm) of catalysts and KIT-6

Catalyst	KIT-6	*Meso*-Mn_2O_3	V–Mn_2O_3	Cu–Mn_2O_3	Mo–Mn_2O_3
Area (m^2 g^{-1})	614	81	46	65	59
Average pore width (nm)	6.6	8.2	6.8	7.6	7.5

3.3.1 *In situ* IR spectra collected in the reaction atmosphere. The FT-IR spectra of the catalysts under the reaction atmosphere (propane : O_2 = 1 : 1) were recorded from 373 to 573 K (Fig. S3†). For *meso*-Mn_2O_3, the 1699 cm^{-1} band at 373 K red-shifted to 1710 cm^{-1} when the temperature increased but vanished at 573 K. This band can be assigned to the $\upsilon_{C=O}$ of acetone coordinated with different Lewis acid sites on the catalyst surface.[20] A new vibration band at 1290 cm^{-1} appears with increasing temperature but disappeared at 573 K. This peak is assigned to carbonate adsorption on the surface of the catalyst and is considered to be a precursor salt of CO_2. Unlike *meso*-Mn_2O_3, the Cu–Mn_2O_3 catalyst showed low reactivity at low temperature (373–473 K). A strong band at 1259 cm^{-1} is detected above 473 K, which means that a large number of carbonate exists. The band at 1650 cm^{-1} is assigned to the physical adsorption of alkenes, indicating that the reaction of propane on Cu–Mn_2O_3 produced propylene or ethylene. The 10% V–Mn_2O_3 and 10% Mo–Mn_2O_3 catalysts exhibit similar absorption spectra and have two weak bands near 1600 cm^{-1} belonging to the Π-bonded propylene species interacting with the Lewis acid sites on the surface of the catalysts. The peak at 1255 cm^{-1} is from the precursor of the carbon oxides. The difference between the V–Mn_2O_3 and the Mo–Mn_2O_3 catalyst is that a vibration peak at 1715 cm^{-1} appears with increasing temperature for 10% V–Mn_2O_3. This implies that the catalytic reaction goes through the acetone step.[21,22]

Fig. 4 compares the FT-IR spectra of the catalysts at 573 K. The CO_2 vibration peak at 2350 cm^{-1} is very strong for *meso*-Mn_2O_3 and the intensity is in the order: *meso*-Mn_2O_3 > Cu–Mn_2O_3 > Mo–Mn_2O_3 > V–Mn_2O_3. These results, combined with the carbonate peak at 1250 cm^{-1}, verified that propane on Cu–Mn_2O_3 and *meso*-Mn_2O_3 produces more CO_2 than that on other catalysts. In addition, the intermediate isopropanol (1065 cm^{-1}) and Π-bonded propene (1600 cm^{-1}) appeared both on V–Mn_2O_3 and Mo–Mn_2O_3, but the acetone peak (1715 cm^{-1}) is only seen on V–Mn_2O_3. These differences illustrate that the oxidation of propane on each catalyst under the reaction atmosphere occurs through two routes. One is mostly complete oxidation to give CO_x, such as that on *meso*-Mn_2O_3 and Cu–Mn_2O_3. The other is primarily selective oxidation to achieve olefins. The isopropanol salt intermediate is further oxidized to acetone and propylene on V–Mn_2O_3 during the reaction, but is further oxidized to propylene and CO_2 on Mo–Mn_2O_3. The Π-bonded propylene was not detected on the *meso*-Mn_2O_3 and Cu–Mn_2O_3 catalysts, but gaseous olefins at 1630 cm^{-1} were detected on Cu–Mn_2O_3. This is inconsistent with the fact that the propylene selectivity is as high as 51% in 10% V–Mn_2O_3. We next studied the adsorption and desorption reaction of propylene on the catalysts to illustrate the huge differences in selectivity between the catalysts.

3.3.2 *In situ* IR of propylene adsorption. Fig. 5 shows the IR spectra of the catalysts after adsorption of propylene at 323 K and their evolution at 373 K. Propylene adsorption on *meso*-Mn_2O_3 was detected at 323 K. The broad vibration peak at 1600 cm^{-1} belongs to the Π-bonded propylene combined with a Lewis acid site, and the shoulder peak at 1630 cm^{-1} is due to the physically adsorbed propylene.[22] A new peak at 1670 cm^{-1} appeared at 373 K, and the intensity of the Π-bonded propene at 1600 cm^{-1} decreased. The peak of 1670 cm^{-1} is regarded as the C=O in aldehyde. This is attributed to the reaction of the Π-bonded propene with the oxide species on the surface of *meso*-Mn_2O_3. This is evidence that propylene is prone to chemisorption on *meso*-Mn_2O_3 with resulting deep oxidation. Propylene adsorption on Cu–Mn_2O_3

Table 2 The performance of the catalysts. Reaction conditions: temperature 480 °C, GHSV = 4500 mL (g h)$^{-1}$, and C_3H_8 : O_2 =1 : 1 (molar ratio)

	Conversion (%)	Selectivity (%)			
Catalyst	Propane	Ethylene	Propylene	CO	CO_2
Meso-Mn_2O_3	24.3	20.6	18.6	0.0	58.2
Bulk-Mn_2O_3	21.1	30.6	22.8	0.0	41.1
10% Mo–Mn_2O_3	22.2	12.0	37.2	11.6	33.0
10% Cu–Mn_2O_3	19.7	12.2	29.5	0.0	56.6
1‰ V–Mn_2O_3	25.7	27.5	17.4	0.0	50.2
1% V–Mn_2O_3	24.4	35.8	28.7	0.0	23.5
5% V–Mn_2O_3	25.6	27.8	31.0	0.0	26.9
10% V–Mn_2O_3	28.8	9.0	51.0	21.1	11.6
15% V–Mn_2O_3	11.9	4.9	41.6	36.4	16.8

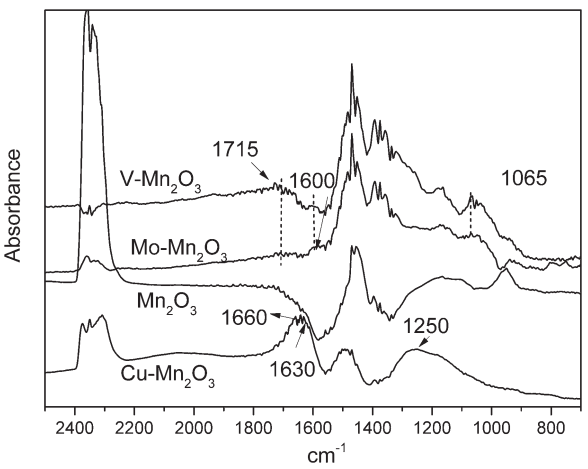

Fig. 4 FT-IR spectra of the reaction atmosphere (propane : O_2=1 : 1) adsorbed on 10% V–Mn_2O_3, 10% Cu–Mn_2O_3, 10% Mo–Mn_2O_3, and *meso*-Mn_2O_3 sample at 573 K.

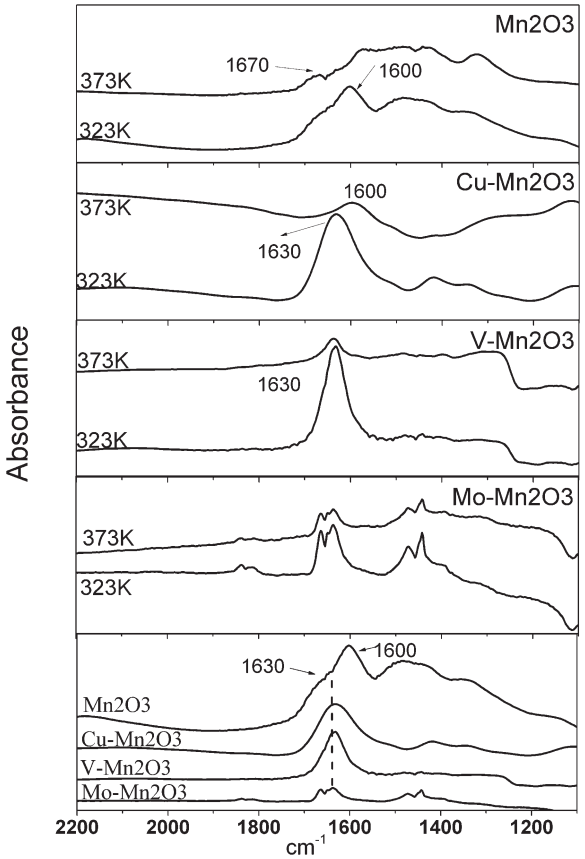

Fig. 5 FT-IR spectra of propylene adsorbed on *meso*-Mn_2O_3, 10% V–Mn_2O_3, 10% Mo–Mn_2O_3, and 10% Cu–Mn_2O_3 from 323 to 373 K, and the comparison of the catalysts at 323 K.

is similar to that on *meso*-Mn_2O_3 at 323 K. The wide peak around 1630 cm^{-1} could include both the vibration of physical adsorption and Π-bonded propylene. After increasing the temperature to 373 K, a sharp peak at 1600 cm^{-1} for the Π-bonded propylene appeared because propylene was easily desorbed. In the spectra of V–Mn_2O_3 and Mo–Mn_2O_3, only the peak of the physically adsorbed propylene (1630 cm^{-1}) remained at 323 K. It is markedly weakened as the temperature increases. When comparing the different catalysts at 323 K (Fig. 5), we see that the intensity of propylene adsorption is of the order: *meso*-Mn_2O_3 > Cu–Mn_2O_3 > V–Mn_2O_3 > Mo–Mn_2O_3. The Π-bonded propylene is seen only on *meso*-Mn_2O_3 and Cu–Mn_2O_3, and its intensity is stronger on *meso*-Mn_2O_3 than on Cu–Mn_2O_3.

The results of the infrared spectra of propylene adsorption on the catalysts show that there are more Lewis acid sites that could easily produce a stable combination with propylene on the surface of Cu–Mn_2O_3 and *meso*-Mn_2O_3. After loading V and Mo, propylene adsorption is decreased. Considering the IR results of (propane + O_2) adsorption, the acid properties of the catalysts affected propylene adsorption–desorption, which in turn determined the selectivity of propylene and CO_x production.

3.3.3 *In situ* IR of NH_3 adsorption. The nature of the acid sites (Lewis and Brønsted) on the surface of the catalysts has been studied by IR spectroscopy, with NH_3 as a probe molecule. The spectra arising from NH_3 adsorption at room temperature followed by evacuation at the same temperature are shown in Fig. 6.

Adsorption of NH_3 on *meso*-Mn_2O_3 leads to the appearance of two strong IR bands at 1425 and 1610 cm^{-1} corresponding to Brønsted (NH_4^+ deformation vibrations) and Lewis acid sites, respectively.[23–25] Adsorption of NH_3 on Cu–Mn_2O_3 shows a strong band centered at 1600 cm^{-1} and two bands from 1350 to 1470 cm^{-1} that could be related to the inhomogeneity of the Brønsted acid sites or a splitting of the δ_{as} vibration due to the adsorption symmetry of the NH_4^+ molecule with the catalyst surface. V–Mn_2O_3 and Mo–Mn_2O_3 show a weak IR band at 1640 cm^{-1} and a medium-strong band at 1420 cm^{-1}. This suggests very little Lewis acid content and dominant Brønsted acids on the surface of these two catalysts. The amount of both Brønsted and Lewis acid sites in the *meso*-Mn_2O_3 and Cu–Mn_2O_3 samples is larger than those in the V–Mn_2O_3 and Mo–Mn_2O_3 samples: *meso*-Mn_2O_3 > Cu–Mn_2O_3 > V–Mn_2O_3 > Mo–Mn_2O_3. The amount of Lewis acid changed more obviously as the dopant changed.

The large number of Lewis acid on *meso*-Mn_2O_3 and Cu–Mn_2O_3 is liable to the adsorbed propylene which then continues to be oxidized to CO_2 in the presence of a Brønsted acid. This caused the selectivity for CO_2 to be greater than 50% on both catalysts. The low amounts of Lewis acid on V–Mn_2O_3 and Mo–Mn_2O_3 allowed propylene to be physically adsorbed and then be desorbed. Thus, both catalysts have higher selectivity for propylene. With increasing V loading, the amount of Lewis acid is significantly reduced, and therefore the selectivity of propylene increased from 17.4 to 51%. Simultaneously, the selectivity of CO is influenced. Too much Lewis acid on *meso*-Mn_2O_3 and Cu–Mn_2O_3 and low loadings (1‰, 1%, and 5%) of V–Mn_2O_3 resulted in no CO production. Increasing the V loadings reduced the Lewis acid

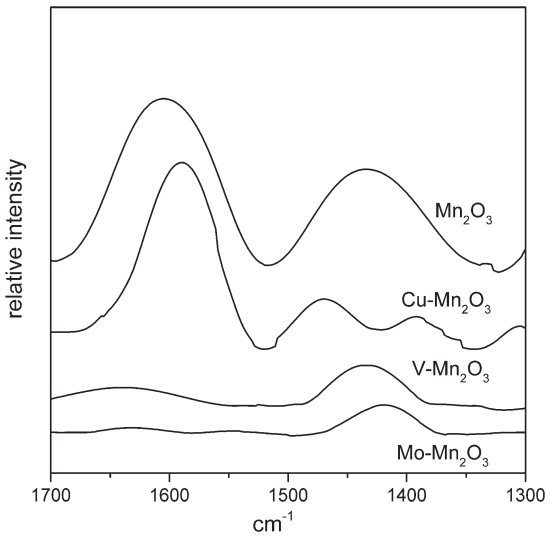

Fig. 6 FT-IR spectra of NH_3 adsorbed and desorbed at room temperature on *meso*-Mn_2O_3, Cu–Mn_2O_3, V–Mn_2O_3, and Mo–Mn_2O_3.

content and increased the CO selectivity to as high as 36.4%. Thus, if a large number of Lewis acid sites exist on the surface of the catalysts, deep oxidation of propane is favorable and the selectivity of CO_2 increases. That is, lower amounts of Lewis acid increase the selectivity for propylene and CO.

3.4 Surface oxygen species

3.4.1 XPS and IR. The composition and oxidation state of the catalysts were confirmed by XPS. The XPS results (Table 3) account for the presence of charged oxygen atoms and hydroxyl oxygen (–OH). On the surface of *meso*-Mn_2O_3, the atomic percentage is 71.99% for O and 28.01% for Mn. These results indicate that the O : Mn atomic ratio (2.57 : 1) is much higher than expected (1.5 : 1) and the test sample exposes oxygen-rich surfaces.

The bulk-Mn_2O_3 sample has a lower O : Mn atomic ratio (2.35 : 1) than *meso*-Mn_2O_3, which indicates the high oxygen capacity of *meso*-Mn_2O_3. The peaks of Mn $2p_{3/2}$ and Mn $2p_{1/2}$ are shown at 642.0 and 653.78 eV, respectively, and the spin–orbit splitting is 11.8 eV. These match well with the data of Mn_2O_3.[26] Two peaks appeared near 531.5 and 529 eV in the XPS profiles of the O 1s region (Fig. S4†) and are attributed to the oxygen (O^{2-}) in the lattice of Mn–O–Mn or the low coordination O^{2-} anions in the bulk (O^{2-}) and to the –OH in the interlayers or on the surfaces, respectively.[27–30] The ratio of the two kinds of oxygen (–OH : O^{2-}) on the surface of *meso*-Mn_2O_3 is the highest (0.774), while that on bulk-Mn_2O_3 is only 0.432. After loading the different elements, the ratio decreases in the order of Cu–Mn_2O_3 > V–Mn_2O_3 > Mo–Mn_2O_3, which is consistent with the changing amounts of Brønsted acid. The ratio of the two kinds of oxygen decreased upon increasing the amount of vanadium loading.

We used *in situ* IR to verify the change in surface –OH. Fig. 7 shows a –OH vibration peak at 3700 cm^{-1} in all the samples. *Meso*-Mn_2O_3 has the maximum number of surface –OH, followed by Cu–Mn_2O_3, V–Mn_2O_3 and Mo–Mn_2O_3. *Meso*-Mn_2O_3 shows a sharp and strong peak of –OH, while the intensity is very weak in bulk-Mn_2O_3. The –OH difference in *meso*- and bulk-Mn_2O_3 was further confirmed by XPS. It is clear that the changes in acidity in the supported catalysts are due to oxygen species on the catalyst surface.

Thus, the Brønsted acids depend on the amount of –OH, which in turn affects propylene selectivity. With differing amounts of V, the Lewis and Brønsted acids decreased with increasing loading, while the propylene selectivity increased from 17.4% to more than 40% and CO_2 decreases significantly. At 10% V, the products are mainly propylene and CO. In short, the surface oxygen species changed the acid properties and thereby affected the reactive products of propane.

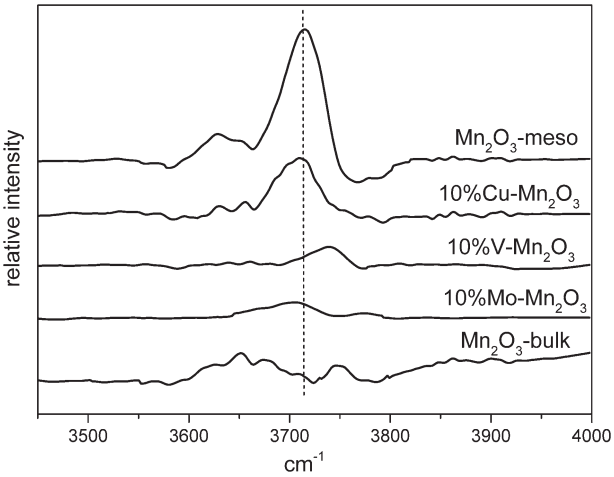

Fig. 7 FT-IR spectra of –OH on the surface of the samples.

3.4.2 The action of oxygen species. To illustrate the role of the oxygen species in the reaction, the adsorption of propane on the catalysts under an oxygen-free atmosphere was measured by *in situ* IR (Fig. 8). *Meso*-Mn_2O_3 and Cu–Mn_2O_3 show a C=C vibration peak near 1580 cm^{-1} at 423 K. The C=O peak at 2400 cm^{-1} is attributed to CO_2 and increases as the temperature increases. For the Cu–Mn_2O_3 catalyst, a peak at 1722 cm^{-1} belongs to acetone vibration and emerges at 373 K; it also increases with increasing temperature. A weak peak of Π-bonded propylene at 1591 cm^{-1} is seen only on V–Mn_2O_3 at elevated temperatures. There is very little CO_2 on V–Mn_2O_3 and Mo–Mn_2O_3 compared to *meso*-Mn_2O_3 and Cu–Mn_2O_3. Mo–Mn_2O_3 did not show any reaction intermediates of propane with increasing temperature. Thus, Mo–Mn_2O_3 does not have catalytic activity for propane under anaerobic conditions.

The reaction intermediate could be compared by the adsorption of propane under aerobic and anaerobic atmospheres on the different catalysts. This relates closely to the different products of propane. The reaction intermediate on *meso*-Mn_2O_3 is not detected except with significant CO_2 under

Table 3 Surface chemical composition of pure Mn_2O_3 and loaded catalysts by XPS[a]

Catalyst	Mn^{3+} (%)	O^{2-} (%)	M^{x+} (%)	O^{2-}/Mn^{3+}	–OH/O^{2-} (area)
Meso-Mn_2O_3	28.0	72.0	0	2.57	0.774
Bulk-Mn_2O_3	29.8	70.2	0	2.35	0.432
10% Mo–Mn_2O_3	22.5	71.7	5.76	3.18	0.428
10% Cu–Mn_2O_3	21.5	69.6	8.85	3.22	0.773
10% V–Mn_2O_3	21.0	71.9	1.63	2.66	0.454
1% V–Mn_2O_3	26.1	73.5	0.43	2.81	0.500
5% V–Mn_2O_3	24.6	74.2	1.15	3.01	0.473
15% V–Mn_2O_3	27.0	70.7	2.34	2.61	0.261

[a] M^{x+}: loaded metal elements.

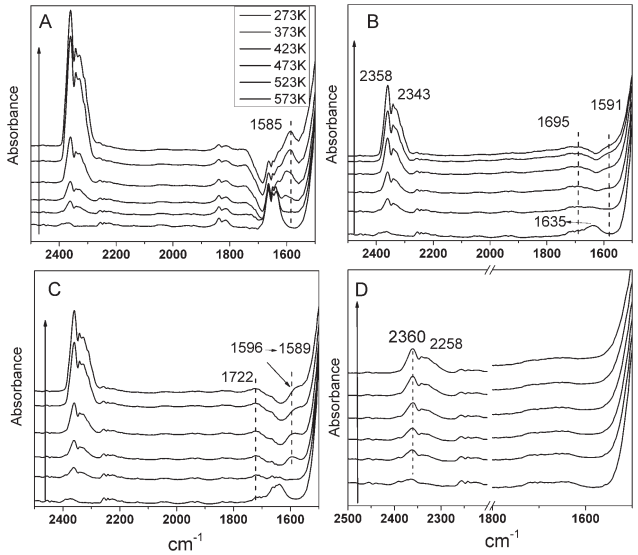

Fig. 8 FT-IR spectra of propane (in the absence of O_2) adsorbed on (A) *meso*-Mn_2O_3, (B) 10% V–Mn_2O_3, (C) 10% Cu–Mn_2O_3 and (D) 10% Mo–Mn_2O_3, from 323 to 573 K.

an aerobic atmosphere. However, the surface oxygen species on *meso*-Mn_2O_3 is involved in the reaction of propane. Here, olefins are generated under anaerobic conditions. Olefins and acetone appeared in the IR spectra of Cu–Mn_2O_3 under the anaerobic atmosphere. On V–Mn_2O_3, the reaction intermediates, propylene and acetone, and a trace of CO_2 were detected under both aerobic and anaerobic conditions. No olefins were detected under anaerobic conditions on Mo–Mn_2O_3, same as under aerobic conditions. The difference in performance under aerobic and anaerobic conditions suggested different exchanges between surface-bound and free oxygen.

The peak near 3800 cm^{-1} is assigned to the –OH vibration on the surface of the catalysts (Fig. S5†). The intensity of the peak decreases gradually as the temperature rises, and the trend is the same for all catalysts, except for Mo–Mn_2O_3. Therefore, the number of –OH on the surface of the catalysts has a great influence on the catalytic reaction of propane. The formation of acetone during propane adsorption suggests that propane is activated by removing a hydrogen atom from the methylene group. This is followed by the bonding of the oxygen species on the catalyst with the nearby secondary carbon of the isopropyl species. This leads to the formation of an isopropoxy species, as shown by Iglesia and coworkers.[31] Thus, when propane is adsorbed, different oxygen species on the surface of the catalysts are prone to oxidation, which is necessary for identification.

3.4.3 CO_2-IR. Infrared spectra recorded following CO_2 adsorption on catalysts at RT and subsequent temperature-programmed desorption are shown in Fig. 9. A number of IR bands from 2000 to 1000 cm^{-1} are observed when CO_2 was adsorbed on the catalysts. This was mainly due to the various types of carbonate-like ($-CO_3$) and bicarbonate ($-HCO_3$) species.[32–36] There are three adsorption situations: the formation of unidentate carbonate, bidentate carbonate and bicarbonate. The formation of unidentate carbonate requires isolated surface O^{2-} ions, *i.e.* low-coordination anions such as those present in corners or edges. Bidentate carbonate forms on the Lewis acid–Brønsted base pairs (M^{2+}–O^{2-} pair site), and the formation of bicarbonate species involves surface hydroxyl groups. The different CO_2 adsorption modes reveal that the surface of the catalysts may contain different oxygen species.

On *meso*-Mn_2O_3, bicarbonates show a C–OH bending mode at 1214 cm^{-1} as well as an asymmetric O–C–O stretching at 1677 cm^{-1}. The intensity of the two peaks decreased with increasing temperature. The C–OH bending mode at 1214 cm^{-1} disappeared at 523 K, indicating that bicarbonate is prone to decomposition. Bidentate carbonate shows symmetric and asymmetric O–C–O vibrations at 1313 and 1627 cm^{-1}, respectively. The intensity of the 1313 cm^{-1} peak decreases slightly with temperatures up to 573 K, indicating that bidentate carbonate is more stable than bicarbonates. Unidentate carbonate shows a vibration peak at 1564 cm^{-1}, which increased with increasing temperature. Among the three adsorption situations for *meso*-Mn_2O_3, the formation of bicarbonate is the most labile. Both the unidentate and bidentate carbonates remain on the surface after evacuation at 573 K. However, only the unidentate band is enhanced with rising temperature. The stability of adsorption suggests that the strength order for the surface sites is as follows: O^{2-} ions > oxygen in M–O pairs > –OH groups.

The adsorption on Cu–Mn_2O_3 also has three carbonate vibrations in the IR (Fig. 9). Bicarbonates show a C–OH bending mode at 1216 cm^{-1}, as well as an asymmetric O–C–O stretching at 1670 cm^{-1}. This shifts to 1681 cm^{-1} at 423 K. Bidentate carbonate vibration appears at 1301 and 1623 cm^{-1}. The peak at 1301 cm^{-1} is stable at 573 K, but the peak at 1623 cm^{-1} vanishes when the temperature rises. Unidentate carbonate shows a vibration peak at 1538 cm^{-1} (asymmetric O–C–O stretching). The mode of the oxide

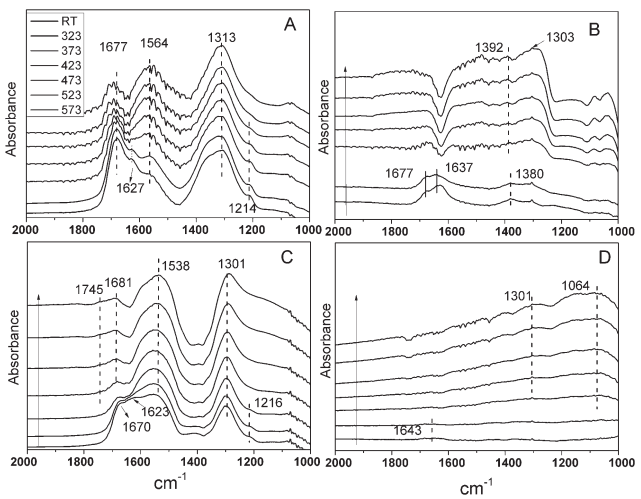

Fig. 9 Infrared spectra of CO_2 adsorbed at 298 K on (A) *meso*-Mn_2O_3, (B) 10% V–Mn_2O_3, (C) 10% Cu–Mn_2O_3 and (D) 10% Mo–Mn_2O_3 taken as a function of temperature during progressive heating under vacuum.

species does not change on the surface of Cu–Mn_2O_3, compared to that on *meso*-Mn_2O_3, but the amount on each mode does change. Bicarbonate species on Cu–Mn_2O_3 is less than that on *meso*-Mn_2O_3, while the unidentate carbonate is much greater on Cu–Mn_2O_3 than on *meso*-Mn_2O_3. Thus, Cu loading increased the isolated surface O^{2-} ions and decreased the –OH group.

The CO_2 adsorption intensity on V–Mn_2O_3 is much weaker than that on Cu–Mn_2O_3. Two peaks appear at 1677 and 1637 cm^{-1} at room temperature and nearly disappear at 373 K. These are the asymmetric O–C–O stretching vibrations of bicarbonates and bidentate carbonates, respectively. The unidentate carbonate shows a weak peak at 1380 cm^{-1} (symmetric O–C–O stretching) and achieves stability at 573 K. The adsorption of CO_2 on Mo–Mn_2O_3 is the weakest in all the catalysts. Weak bidentate carbonate appeared at 1643 cm^{-1} and vanished with increasing temperature. No bicarbonates and unidentate carbonates were detected. These results also suggest the following content order for OH groups: *meso*-Mn_2O_3 > Cu–Mn_2O_3 > V–Mn_2O_3 > Mo–Mn_2O_3. For O^{2-} ion groups, the trend is: Cu–Mn_2O_3 > *meso*-Mn_2O_3> V–Mn_2O_3 > Mo–Mn_2O_3, and for oxygen in M–O pairs: *meso*-Mn_2O_3 > Cu–Mn_2O_3 > V–Mn_2O_3 > Mo–Mn_2O_3. The order for –OH groups is consistent with the results of XPS and IR.

In summary, the amount of –OH oxide species (–HCO_3) is the same as that of the Brønsted acid. This shows that the amount of Brønsted acid on the catalysts is completely determined and controlled by these oxygen species. From the association with the catalytic properties, it can be seen that this kind of oxygen species (*i.e.*, Brønsted acid) mainly undergoes a deep oxidation process during propane oxidation and generates CO_2. It has been shown from the results of NH_3-IR and CO_2-IR that the change in Mn^{3+}–O^{2-} pairs is the same as that in the Lewis acid. Thus, the Lewis acid–base pairs of Mn^{3+}–O^{2-} on the surface of the catalysts are deemed to form Lewis acid sites. The decrease in Lewis acid–base pairs decreases the number of Lewis acid sites when the V content increases from 0.01 to 0.15. Meanwhile, the selectivity of CO_2 drops from 50.2 to 16.8%, and the selectivity of propylene rises from 17.4 to 50%. Although it could not be proven that propane on the Lewis acid–base pairs (Lewis acid sites) also generates CO_2, it is clear that a small amount of the Lewis acid–base pairs is unfavorable for CO_2 generation, but advantageous for propylene production.

When comparing V–Mn_2O_3 and Mo–Mn_2O_3 catalysts, it can be observed that they have nearly the same amount of –OH (Brønsted acid) from the results of IR and NH_3-IR, but have a big difference in propylene selectivity because the oxide species of Mn^{3+}–O^{2-} pairs (Lewis acid sites) on V–Mn_2O_3 is more than that on Mo–Mn_2O_3. That is to say, a certain amount of Mn^{3+}–O^{2-} pairs favors propylene during propane oxidation.

Conclusions

Meso-Mn_2O_3 was loaded with different elements (V, Mo and Cu) to change the acid properties of the catalysts and further influence the catalytic reaction pathways of the probe molecule (propane). A large number of Brønsted acids (controlled by –OH) exist on the surface of the catalysts (*meso*-Mn_2O_3, Cu–Mn_2O_3). Brønsted acids mainly go through the deep oxidation process during propane oxidation and are conducive to the generation of CO_2. Lower amounts of Lewis acids are advantageous to the selectivity of propylene and CO. The surface oxygen species were detected by XPS and CO_2-IR. A small amount of the Lewis acid–base pairs decreases CO_2 generation, but is advantageous for propylene. This implies that Mn^{3+}–O^{2-} could be considered to form the Lewis acid sites. Different oxygen species play different roles in propane oxidation as propane molecules could undergo selective oxidation or complete oxidation reactions. Thus, these results provide a basis for managing the complete or selective oxidation of light alkanes by adjusting the surface oxygen species.

Acknowledgements

The authors are grateful for the financial support from the National Natural Science Foundation of China (grant no. 21173186).

Notes and references

1 M. A. Hasan, M. I. Zaki and L. Pasupulety, *J. Phys. Chem. B*, 2002, **106**, 12747.
2 V. P. Santos, M. F. R. Pereira, J. J. M. Orfao and J. L. Figueiredo, *Appl. Catal., B*, 2009, **88**, 550.
3 Y. Liu, X.-S. Li, C. Shi, J.-L. Liu, A.-M. Zhu and B. W. L. Jang, *Catal. Sci. Technol.*, 2014, **4**, 2589.
4 H. Li, G. Qi, Tana, X. Zhang, W. Li and W. Shen, *Catal. Sci. Technol.*, 2011, **1**, 1677.
5 J. Verhelst, D. Decroupet and D. De Vos, *Catal. Sci. Technol.*, 2013, **3**, 1579.
6 M. Baldi, V. S. Escribano, J. M. G. Amores, F. Milella and G. Busca, *Appl. Catal., B*, 1998, **17**, L175.
7 S. J. A. Figueroa, F. G. Requejo, E. J. Lede, L. Lamaita, M. A. Peluso and J. E. Sambeth, *Catal. Today*, 2005, **107–08**, 849.
8 S. L. Suib, *J. Mater. Chem.*, 2008, **18**, 1623.
9 M. A. Peluso, E. Pronsato, J. E. Sambeth, H. J. Thomas and G. Busca, *Appl. Catal., B*, 2008, **78**, 73.
10 M. Baldi, E. Finocchio, C. Pistarino and G. Busca, *Appl. Catal., A*, 1998, **173**, 61.
11 M. Che and A. J. Tench, *Adv. Catal.*, 1982, **31**, 77.
12 M. Che and A. J. Tench, *Adv. Catal.*, 1983, **32**, 1.
13 P. J. Gellings and H. J. M. Bouwmeester, *Catal. Today*, 1992, **12**, 1.
14 S. Chen, F. Ma, A. X. Xu, L. N. Wang, F. Chen and W. M. Lu, *Appl. Surf. Sci.*, 2014, **289**, 316.
15 X. T. Gao, J. L. G. Fierro and I. E. Wachs, *Langmuir*, 1999, **15**, 3169.
16 S. Rajagopal, J. A. Marzari and R. Miranda, *J. Catal.*, 1995, **151**, 192.
17 F. Kleitz, S. H. Choi and R. Ryoo, *Chem. Commun.*, 2003, 2136.

18 F. Jiao, A. Harrison, A. H. Hill and P. G. Bruce, *Adv. Mater.*, 2007, **19**, 4063.
19 V. Escax, M. Imperor-Clerc, D. Bazin and A. Davidson, *C. R. Chim.*, 2005, **8**, 663.
20 X. D. Yi, X. B. Zhang, W. Z. Weng and H. L. Wan, *J. Mol. Catal. A: Chem.*, 2007, **277**, 202.
21 A. A. Davydov, V. G. Mikhaltchenko, V. D. Sokolovskii and G. K. Boreskov, *J. Catal.*, 1978, **55**, 299.
22 P. Concepcion, P. Botella and J. M. L. Nieto, *Appl. Catal., A*, 2004, **278**, 45.
23 W. M. Zhang, P. G. Smirniotis, M. Gangoda and R. N. Bose, *J. Phys. Chem. B*, 2000, **104**, 4122.
24 P. G. Smirniotis, P. M. Sreekanth, D. A. Pena and R. G. Jenkins, *Ind. Eng. Chem. Res.*, 2006, **45**, 6436–6443.
25 A. M. Venezia, L. Palmisano, M. Schiavello, C. Martin, I. Martin and V. Rives, *J. Catal.*, 1994, **147**, 115.
26 H. Q. Dong, Y. Y. Chen, M. Han, S. L. Li, J. Zhang, J. S. Li, Y. Q. Lan, Z. H. Dai and J. C. Bao, *J. Mater. Chem. A*, 2014, **2**, 1272.
27 M. I. Zaki, M. A. Hasan, L. Pasupulety and K. Kumari, *New J. Chem.*, 1998, **22**, 875.
28 W. S. Choi, *Electron. Mater. Lett.*, 2012, **8**, 87.
29 N. Ohno, Y. Akeboshi, M. Saito, J. Kuwano, H. Shiroishi, T. Okumura and Y. Uchimoto, *Top. Catal.*, 2009, **52**, 903.
30 X. J. Yang, Y. Makita, Z. H. Liu, K. Sakane and K. Ooi, *Chem. Mater.*, 2004, **16**, 5581.
31 K. D. Chen, A. T. Bell and E. Iglesia, *J. Catal.*, 2002, **209**, 35.
32 V. K. Diez, C. R. Apesteguia and J. I. Di Cosimo, *Catal. Today*, 2000, **63**, 53.
33 N. Hiyoshi, K. Yogo and T. Yashima, *Microporous Mesoporous Mater.*, 2005, **84**, 357.
34 A. C. C. Chang, S. S. C. Chuang, M. Gray and Y. Soong, *Energy Fuels*, 2003, **17**, 468.
35 K. Pokrovski, K. T. Jung and A. T. Bell, *Langmuir*, 2001, **17**, 4297.
36 W. G. Su, J. Zhang, Z. C. Feng, T. Chen, P. L. Ying and C. Li, *J. Phys. Chem. C*, 2008, **112**, 7710.